Optimal Placement of Individual LF Antennas on Each Axis in a Small Mobile Device Through a Systematic Optimization Process

Tae Heung Lim, Jun Hur, and Hosung Choo

***Abstract*—This letter proposes the optimal placement of individual low-frequency (LF) antennas on each axis integrated in a small mobile device platform to maximize the coverage range of the communication link. To achieve the maximum coverage, considering small platform effects, a systematic genetic algorithm optimization process was conducted using a readable volume metric as a cost function. A readable volume of 34.5 m^3 at the optimum locations of the individual LF antennas was obtained compared with that of 21.6 m^3 for the bundle of LF antennas. To verify the results, Poynting vector measurements were performed using LF antennas located at optimal positions inside the copper mobile device platform. The Poynting vector strengths at the range of 30 cm were −138.9, −140.7, and −138.7 dBW/m^2 along the *x*-, *y*-, and *z*-axis, respectively.**

***Index Terms*—Low-frequency (LF) antenna, passive access system entry (PASE), position optimization, small mobile device.**

I. Introduction

In RECENT years, the use of smart key systems that adopt various wireless systems, such as the hands-free system, remote keyless entry, and the passive access system entry (PASE), has been drastically expanded [1]–[5]. In particular, the PASE system allows users to open car doors, start engine ignitions, and control automatic parking systems while keeping one's car keys in one's pocket. In order to achieve these features, highly-sensitive antennas are essential for both the user and the vehicle to maintain a stable wireless communication link through a strong near magnetic field. The antenna used in the PASE system usually operates in the low-frequency (LF) band at 125 kHz for high penetration and low transmission loss characteristics with a large wavelength. The LF antenna is typically composed of a ferrite core and a conducting wire wound around the core with multiple turns. When an LF antenna is mounted onto a smart key or small-mobile device, the resulting magnetic field generated by the antenna should have a semiuniform amplitude distribution with proper polarizations along the *x*-, *y*-, and *z*-axis to create a stable communication link and an increased coverage range of the PASE system. To obtain a better coverage range, three individual bar-type LF antennas are usually integrated into a bundle to produce an omnidirectional-field pattern [6]. Recently, a three-axis LF antenna with a single ferrite core and conducting wires wound along the three axes was introduced [7]. In addition, studies on the coverage range estimation of a large platform were carried out to demonstrate the performance of the PASE system depending on the locations of the LF antennas inside the vehicles [8]–[10]. These studies focused on improving the performance of the bundled LF antennas integrated in the module, but did not significantly consider the range variation depending on various mounting positions and the near-field pattern distortions due to the small platform effect.

In this letter, we propose the optimal placement of individual LF antennas on each axis mounted on a small mobile device to maximize the coverage range of the communication link. The systematic optimization process is developed using a readable volume metric as a cost function to achieve the maximum coverage, considering small platform effects. Three LF antennas are used to operate in the *x*-, *y*-, and *z*-polarization, which consists of a cuboid or cylindrical ferrite core and a conducting coil. To estimate the optimal positions, the LF antennas and the small mobile device are modeled using the FEKO electromagnetic (EM) simulation software [11]. Here, the size of the small mobile device should have enough available space to adjust the positions of the LF antennas, otherwise the position optimization effect may be negligible. A genetic algorithm (GA) was employed in our systematic optimization process, and the readable volume metric used as the cost function is calculated based on each position of the three LF antennas. We then compare the measured Poynting vectors for the LF antennas mounted on the mobile device with the simulation. The results confirm that position optimization of the individual antennas for each axis in the small mobile platform is essential in maximizing the coverage range.

II. Systematic Optimization for Individual LF Antennas

A. EM Modeling and Optimization Process

Fig. 1 shows a conceptual illustration of the difference between the positioning method of the LF three-axis antenna

Manuscript received October 10, 2019; revised November 5, 2019; accepted November 14, 2019. Date of publication November 25, 2019; date of current version January 20, 2020. This work was supported in part by the Basic Science Research Program through the National Research Foundation of Korea (NRF) funded by the Ministry of Education under Grants 2015R1A6A1A03031833 and NRF-2017R1D1A1B04031890 and in part by the NRF grant funded by the Korea government (MSIP) under Grant NRF-2017R1A5A1015596. *(Corresponding author: Jun Hur.)*

T. H. Lim and H. Choo are with the School of Electronic and Electrical Engineering, Hongik University, Seoul 04066, South Korea (e-mail: qpzm_0105@naver.com; hschoo@hongik.ac.kr).

J. Hur is with the Metamaterial Electronic Device Research Center, Hongik University, Seoul 04066, South Korea (e-mail: gjwns0@naver.com).

Digital Object Identifier 10.1109/LAWP.2019.2955457

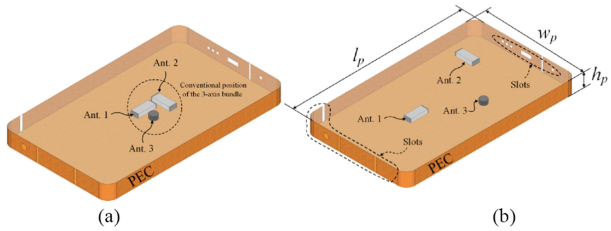

Fig. 1. LF antenna positioning methods in a small mobile device. (a) Position optimization of the three-axis antenna bundle. (b) Position optimization of individual antennas on each axis.

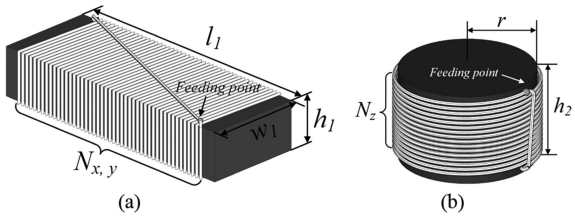

Fig. 2. Two types of LF antennas. (a) Cuboid-shape LF antenna. (b) Cylindrical-shape LF antenna.

TABLE I
DETAILED PARAMETERS OF THE PROPOSED ANTENNA AND THE PLATFORM

Parameters	Values
w_1	3.55 mm
l_1	11.4 mm
h_1	2.35 mm
r	5.3 mm
h_2	2.35 mm
w_p	68.8 mm
l_p	145.8 mm
h_p	7.9 mm
$N_x = N_y = N_z$	200 turns

bundle and a positioning method of individual LF antennas on each axis in a small mobile device. In the conventional method, three LF antennas are bundled together in one place, whereas in the proposed method, individual LF antennas are arranged at arbitrary positions in the platform. To optimize the positions of the three LF antennas, we modeled two types of commercial LF antennas and the platform of the mobile device using FEKO EM simulation software, as can be seen in Fig. 2. The first type of antenna has a cuboid ferrite core with dimensions of $w_1 \times l_1 \times h_1$ mm^3 and is wound by coils with N_x or N_y turns to operate with x- and y-polarization. The second type of antenna consists of a cylinder shape ferrite core, with a radius of r, a height of h_2, and a coil with N_z turns to concentrate the magnetic flux density along the z-axis. These antennas are mounted onto a small mobile device platform, which consists of a thin deltahedron with rectangular surfaces of perfect electric conductor. This platform, with dimensions of $w_p \times l_p \times h_p$ mm^3, also has various slots on the sides for speakers, an ear jack, and a charging jack. All detailed values of the parameters are listed in Table I. Fig. 3 presents a flowchart of the systematic optimization process for the individual LF antennas on each axis. To optimize the positions of the individual LF antennas, the small mobile platform is virtually divided into 7 × 9 grid areas in the xy plane with position numbers from P_{11} to P_{79}, where the first

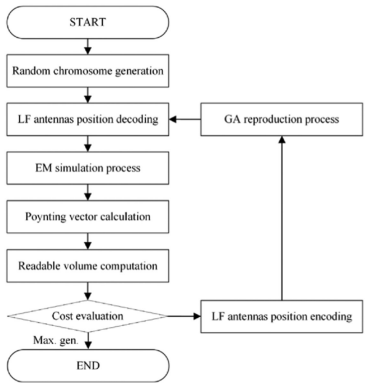

Fig. 3. Flowchart of the systematic optimization process for the individual antennas on each axis.

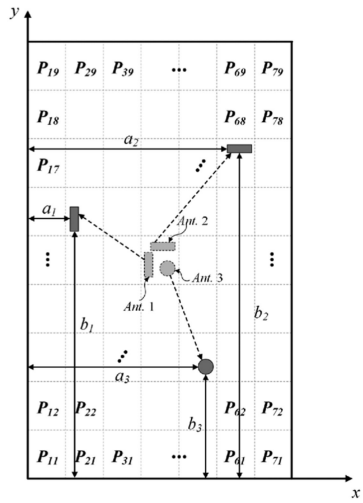

Fig. 4. 7 × 9 grid areas on the platform to optimize the positions of the individual LF antennas on each axis.

and second subscripts indicate grid numbers along the x- and y-direction, as shown in Fig. 4. Each grid area can contain all of the LF antennas without overlapping with each other, and Ant. n is set by variables of a_n and b_n $(n = 1, 2, 3)$. While employing GA as an optimization algorithm, in the first process, initial chromosomes consisting of binary bits are randomly generated to decode the positions for the individual antennas. Next, the individual LF antennas are placed at the initial positions in the small mobile device and are simulated to obtain the electric and magnetic near-field distributions (-3 m $\leq x, y, z \leq 3$ m, 41 × 41 × 21 points)

$$P(x, y, z) = \frac{1}{2}\mathrm{Re}\left\{\bar{E}(x, y, z) \times \bar{H}^*(x, y, z)\right\}. \quad (1)$$

The Poynting vectors are then calculated from the resulting near-field distributions at each point by (1), and the calculated Poynting vector datasets are uniformly extended to 401 × 401 points in the xy plane. The readable volume of the system is then obtained and used as the cost function for the GA process, which is defined as follows:

$$V_{\mathrm{read}} = \int_{z=-L}^{L} \int_{\phi=0}^{2\pi} R(\phi, z)\, d\phi dz \quad (2)$$

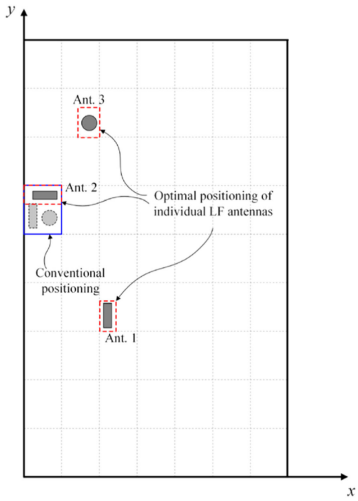

Fig. 5. Optimum positions of a bundled LF antenna and individual LF antennas.

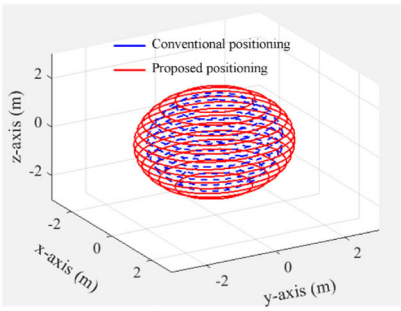

Fig. 6. Real 3-D readable volumes for the optimized positions of the bundled LF antennas and the individual LF antennas.

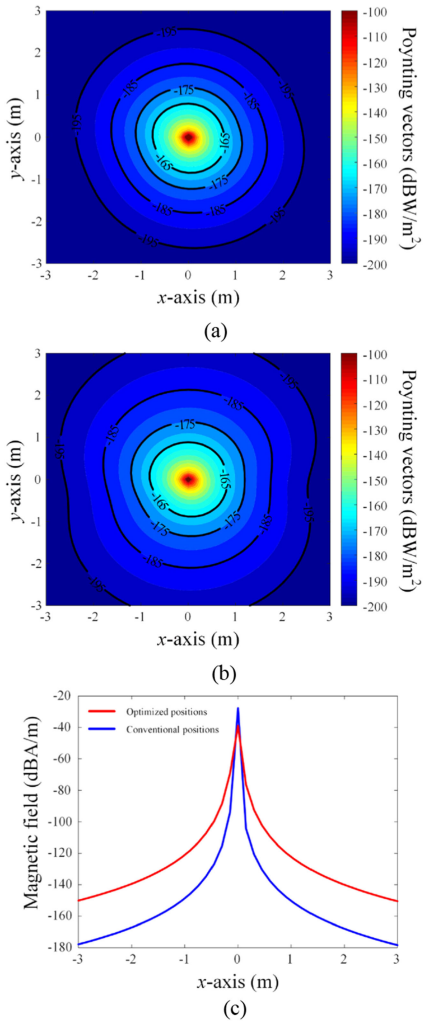

Fig. 7. Power density and magnetic field distributions. (a) Conventional bundled LF antennas ($z = 0$ m). (b) Individual LF antennas at optimized positions ($z = 0$ m). (c) Magnetic field comparison between conventional bundled LF antennas and individual LF antennas at optimized positions (y and $z = 0$ m).

where $R(\phi, z)$ is the maximum readable distance with the Poynting vector $P(r, \phi, z)$ above a threshold Poynting vector strength of P_{Th}. L is the maximum height along the z-axis, and V_{read} indicates the readable volume. The threshold Poynting vector strength P_{Th} of -185 dBW/m^2 is appropriately determined through the experimental result. Then, V_{read} is obtained for the cost evaluation by the summation of the area, which is calculated from the integration of $R(\phi, z)$ within $0 < \phi < 2\pi$ and $-L < z < L$. After the cost evaluation, the information on the three LF antenna positions is encoded into binary numbers to apply it to the GA reproduction process of the crossover and mutation. The GA process is repeated for 25 generations with 40 populations. Therefore, a total of 1000 samples are evaluated to achieve the enhanced readable volume. To compare with the conventional positioning, the bundle of the LF antennas is simulated in all grid areas, and the best result of the readable volume is chosen and compared against the optimum GA result. Fig. 5 illustrates the optimized positions for the conventional and proposed positioning methods. The optimum position of the bundled LF antennas is chosen at the grid area of P_{17}, and the locations for the individual LF antennas Ant. 1, 2, and 3 are placed at the points of P_{17}, P_{54}, and P_{27}. Each optimum position is specified by a blue solid-line box and red dotted-line box, respectively. Fig. 6 shows the resulting three-dimensional (3-D) readable volumes obtained within P_{Th} according to the x-, y-, and z-coordinate. The positioning method of the individual LF antennas has a readable volume of 34.5 m^3 compared with that of 21.6 m^3 for the conventional bundled LF antennas. These results confirm that the proposed individual LF antenna positioning method of the systematic optimization process has a better performance in terms of achieving the communication link in the readable range than the conventional positioning method.

Fig. 7(a) and (b) illustrates the reading range depending on the minimum required Poynting vector strengths of the transponders. The results demonstrate that the optimized positions of the LF antennas have higher reading range compared with the conventional positions of the bundled LF antennas. For the field analysis, we simulate the magnetic field distributions in a distance up to 3 m along the x-axis (y and $z = 0$ m) to observe the merit of the optimized position of the LF antennas compared with the conventional bundled LF antennas, as can be seen in Fig. 7(c). The results show that the proposed design

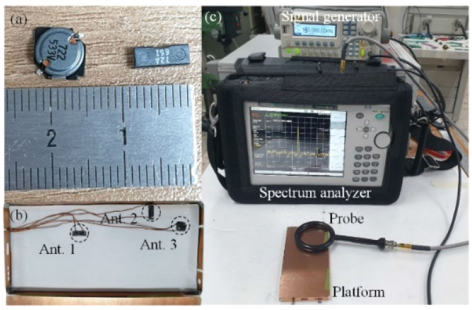

Fig. 8. Measurement setup for the individual LF antennas at the optimum positions in a small mobile device platform. (a) Two types of commercial LF antennas. (b) Optimum placement in the platform. (c) Measurement setup.

has a stronger magnetic field level than the conventional design after 10 cm. At the distance of 2 m, the magnetic field of the individual LF antennas at the proposed positions is 30 dB higher than that of the conventional bundled LF antennas. These results demonstrate that the proposed individual LF antenna positioning method of the systematic optimization process can have the higher power density and larger reading ranges than the conventional positioning method because each LF antenna is separated in some distances that could reduce mutual couplings and platform effects.

B. Measurement of Optimal Positions for LF Antennas

Fig. 8 shows the measurement setup for the individual LF antennas at the optimum positions in a small mobile device platform. The Poynting vectors are measured using bar and cylindrical types of commercial LF antennas (Murata 1143AA, 1312AA) located at the optimized positions and the conventional bundled positions inside the small mobile device platform composed of copper plates. All three LF antennas are then excited by a signal generator at 125 kHz frequency with a voltage of 12 V, and an ETS-Lindgren EM-6992 magnetic probe is used to receive the Poynting vector strengths along the x-, y-, and z-axis (-30 cm $\leq x, y \leq 30$ cm, and $0 \leq z \leq 30$ cm) using an Anritsu MS2720T spectrum analyzer. The LF antennas are measured to have x-, y-, and z-component of the Poynting vector strengths at each measurement point to sum up all of the components. Fig. 9 depicts the measured and simulated Poynting vector strengths of the individual LF antennas at optimum postions indicated by red circles and red lines, respectively, and those of the conventional bundled LF antennas specified by blue squares and blue lines in the the x-, y-, and z-direction. The Poynting vector strengths of the proposed design at a distance of 30 cm are -138.9, -140.7, and -138.7 dBW/m^2 along the x-, y-, and z-axis, respectively, and both simulated and measured results have similar Poynting vector strength trends. Therefore, we confirm that the proposed positioning method has a Poynting vector strength of 4.1 dB higher than the conventional method at the distance of 30 cm on the z-axis. According to these results, the systematic optimization process is suitable to achieve the maximum readable volume for locating the three individual LF antennas.

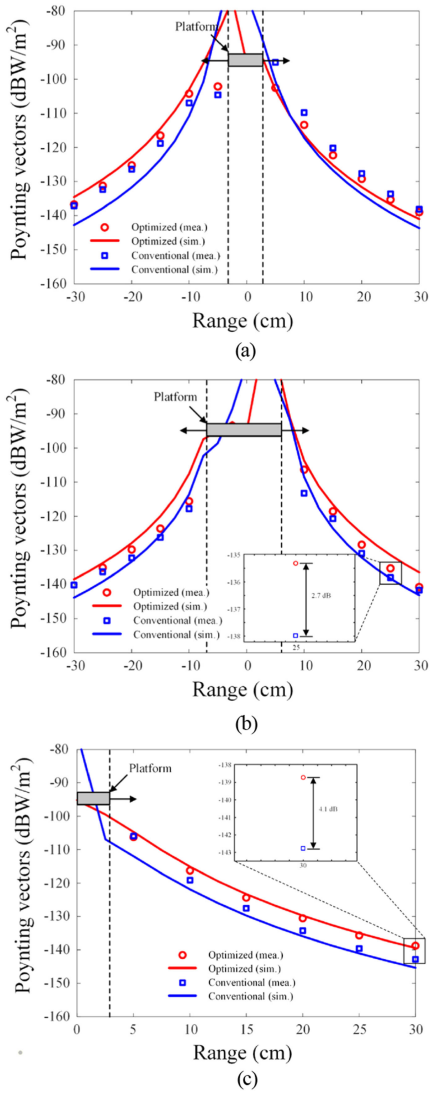

Fig. 9. Measured and simulated results of the individual LF antennas at the optimum positions and the conventional bundled positions in a small mobile device platform along three axes. (a) x-axis. (b) y-axis. (c) z-axis.

III. Conclusion

The systematic method for positioning individual LF antennas on a small mobile device platform was proposed to enhance the coverage range of the communication link. In the employed GA process, a readable volume metric was used as a cost function to achieve the maximum coverage, considering small platform effects. Through the optimization process, the optimum locations of the individual LF antennas had a readable volume of 34.5 m^3 compared with that of 21.6 m^3 for the conventional bundled antenna positioning method. To confirm the results, Poynting vectors measurements were obtained using commercial LF antennas located at the optimal positions inside the platform. The Poynting vector strengths at the range of 30 cm were -138.9, -140.7, and -138.7 dBW/m^2 along the x-, y-, and z-axis, respectively. According to these results, the systematic optimization process is suitable to achieve the maximum readable volume for locating the three individual LF antennas.

REFERENCES

[1] A. Takacs, M. Huard, S. Kessler, G. A. Chakam, and E. Lardjane, "Estimation of low frequency coverage inside car for passive access system entry," *Electron. Lett.*, vol. 45, no. 12, pp. 596–597, Jun. 2009.

[2] M. Heddebaut, V. Deniau, and K. Adouance, "Invehicle WLAN radio frequency communication characterization," *IEEE Trans. Intell. Transp. Syst.*, vol. 5, no. 2, pp. 114–121, Jun. 2004.

[3] M. Hirano, M. Takeuchi, and T. Tomoda, and K.-I. Nakano, "Keyless entry system with radio card transponder [automobiles]," *IEEE Trans. Ind. Electron.*, vol. 35, no. 2, pp. 208–216, May 1988.

[4] K. Keum, H. Piao, and J. Choi, "Design of a short/open-ended slot antenna with capacitive coupling feed strips for hepta-band mobile application," *J. Electromagn. Eng. Sci.*, vol. 18, no. 1, pp. 46–51, Jan. 2018.

[5] S. Lee, H. Yoon, K. Baik, and B.-J. Jang, "Emulator for generating heterogeneous interference signals in the Korean RFID/USN frequency band," *J. Electromagn. Eng. Sci.*, vol. 18, no. 4, pp. 254–260, Oct. 2018.

[6] K. Sato and K. Sano, "3D receptive ultrathin LF band antenna," in *Proc. IEEE 3rd Global Conf. Consum. Electron.*, Oct. 2014, pp. 422–425.

[7] S. T. G. Maguire, P. A. Robertson, and B. Smith, "Low frequency radio polarization sensor with applications in attitude estimation," *IEEE Sensors J.*, vol. 15, no. 12, pp. 7304–7311, Dec. 2015.

[8] K. J. Hawes, F. B. Woloch, S. N. Rohr, and J. A. Hite, "Receiver for an automotive remote keyless entry system," European Patent EP 0903456 A1, Aug. 1998.

[9] J. Goings, T. Prescott, and P. Lepek, "Optimizing passive keyless entry system performance," *Automobile Compilation*, vol. 8, pp. 23–29, Jan. 2011.

[10] H. Kim, G. Byun, J. Seong, H. Jung, and H. Choo, "Near-field analysis of vehicle LF antennas for estimating the reading range of a smart key," *J. Korean Inst. Electromagn. Eng. Sci.*, vol. 24, no. 7, pp. 671–677, Jul. 2013.

[11] FEKO EM Simulation Software, Altair Engineering Inc., Troy, MI, USA, 2019. [Online]. Available: http://www.altair.co.kr